RSC Advances

PAPER

View Article Online
View Journal | View Issue

Cite this: *RSC Adv.*, 2020, **10**, 10689

Biomass-derived Fe-NC hybrid for hydrogenation with formic acid: control of Fe-based nanoparticle distribution†

Lu Liu,‡[a] Bowei Wang, ‡[abc] Ruixiao Gao,[a] Dan Zhang,[a] Wensheng Xu,[a] Ligong Chen, *[abc] Xilong Yan [abc] and Yang Li *[abc]

Received 12th February 2020
Accepted 6th March 2020

DOI: 10.1039/d0ra01356k

rsc.li/rsc-advances

A series of Fe-NC catalysts were synthesized by pyrolyzing an Fe complex and wheat flour at 500 °C. All of them were characterized and applied in the catalytic transfer hydrogenation of nitroarenes with formic acid. It was found that the catalytic activity was significantly affected by the size and distribution of Fe-based nanoparticles (NPs), which could be easily regulated by altering the Fe source. Meanwhile, more basic nitrogen sites were preserved on the catalyst so that the reaction ran smoothly without base additives. Among all catalysts, Fe-NC-$FeCl_2$ exhibited the best catalytic performance due to smaller Fe_3O_4 NPs and greater N doping. Moreover, it showed excellent applicability for diverse nitroarenes. Obviously, this work demonstrates the importance of the metallic NPs' size and distribution, providing a new insight into the design of M-NC catalysts. The catalyst is economical and eco-friendly, and shows potential application value in industry.

Introduction

Aniline and its derivatives are important building blocks and intermediates in bulk and fine chemicals, and mainly obtained by selective reduction of nitroarenes.[1–4] Traditional industrial reduction methods with iron powder or sodium sulfide are deprecated in industry due to serious pollution.[5,6] Instead, catalytic hydrogenation and catalytic transfer hydrogenation (CTH) are regarded as ideal candidates for nitroarene reduction. Catalytic hydrogenation undoubtedly has the advantages of high atom utilization but also inevitably brings dangers of high temperature and pressure as well.[7,8] Fortunately, the CTH method, in which the hydrogen supply reagent, such as, $NH_3 \cdot BH_3$,[9] HCOOH (FA),[10,11] and isopropyl alcohol,[12] is used as a reductant, could overcome the disadvantages of catalytic hydrogenation in view of the mild reaction conditions, safe and simple process, *etc.* Compared with other reductants, FA, with great application prospects in hydrogen generation, is nontoxic, renewable and easily available.[13]

In the CTH process, the catalyst is of vital importance. In the past decade, noble metal catalysts had been extensively studied, showing high activity.[14–16] However, high price and scarcity of precious metal seriously restrict the large-scale use and go against the idea of sustainable development. Therefore, transition metal-based (*e.g.*, Fe, Co and Ni) heterogeneous catalysts are actively explored to replace the precious metal catalysts. It is worth mentioning that Fe is an ideal choice in virtue of the lowest price and eco-friendliness among all non-noble metals.[2,17] Unfortunately, the performance of Fe-based catalysts is far from being satisfactory in comparison to other non-noble metal catalysts.

In 2013, Beller and co-workers developed a novel Fe-NC catalyst with Fe_2O_3 particles embedded in nitrogen-doped carbon layers by pyrolysis of iron–phenanthroline complex on carbon (Vulcan XC72R).[18] It was successfully applied in the CTH of nitrobenzene by FA in the presence of triethylamine.[19] Henceforth, the M-NC (M = Fe, Co, Ni or their oxide) catalysts have emerged as a new class of transition metal-based catalysts due to high activity and selectivity,[20] low metal loading, as well as the excellent stability. Nevertheless, there are still some limitations about M-NC catalysts. For instance, high temperature pyrolysis would result in the agglomeration of metal nanoparticles (NPs). Consequently, the as-synthesized catalysts generally suffer from nonuniform dispersion of metal NPs owing to uncontrollable pyrolysis process,[21] which dramatically restrains the enhancement of catalytic activity. In some cases, acid etching is employed to remove large metal NPs to promote catalytic activity,[22] but this strategy is not eco-friendly. Thus, exploring effective strategies to control the NPs' size and distribution of M-NC catalyst is still a challenge. In our recent study, it

[a]*School of Chemical Engineering and Technology, Tianjin University, Tianjin 300350, P. R. China. E-mail: lgchen@tju.edu.cn; liyang777@tju.edu.cn*

[b]*Collaborative Innovation Center of Chemical Science and Engineering (Tianjin), Tianjin 300072, P. R. China*

[c]*Tianjin Engineering Research Center of Functional Fine Chemicals, Tianjin, P. R. China*

† Electronic supplementary information (ESI) available. See DOI: 10.1039/d0ra01356k

‡ These authors contributed equally to this work.

was found that Co salts could regulate the NPs size of Co-NC catalyst and further impact their activity.[23] However, as for Fe-NC catalyst, some previous works reported that the change of the Fe source could significantly deactivate the catalyst despite the change of the catalyst morphology.[24] In addition, high pyrolysis temperature about 800 °C is usually required to optimize catalytic activity in most reported literature.[25–27]

Harsh preparation condition limits the development of these novel catalysts, because the size and distribution of metal-based NPs are uncontrollable. In our previous work, Fe-NC catalyst was successfully synthesized at 500 °C, which exhibited good activity for catalytic hydrogenation. Although many small Fe-based NPs with the size of 2–10 nm were found, there were still many large NPs (100–180 nm).[28]

In this work, we want to establish a novel strategy to construct highly-dispersed Fe-NC catalyst by pyrolyzing Fe complex and biomass carbon source at low temperature. On the one hand, the low pyrolysis temperature is in favor of the size and distribution of Fe-based NPs. Meanwhile, the NPs size was tried to regulate by changing the Fe salts. Moreover, the low pyrolysis temperature is also beneficial to doping N in the carbon matrix as pyridinic N species,[29] which can serve as co-catalyst to promote the decomposition of O–H bond in FA due to the Lewis basicity and avoid the addition of basic assistant.[30,31] The as-synthesized catalysts were characterized by XRD, Raman, SEM, TEM, N_2 adsorption–desorption measurement, ICP-OES, elemental analysis, and XPS. Their activity was evaluated by the CTH of nitrobenzene using FA as reductant. The structure–activity relationship was discussed in detail. Furthermore, the general applicability of the catalyst was also explored.

Experimental

Catalysts preparation

The following iron salts were utilized respectively in the preparation of the Fe-based catalysts: $FeCl_2 \cdot 4H_2O$, $FeCl_3 \cdot 6H_2O$, $FeSO_4 \cdot 7H_2O$, $Fe(NO_3)_3 \cdot 9H_2O$ and $Fe(acac)_3$. Take Fe-NC-$FeCl_2$ as an example, $FeCl_2$ was dissolved in 40 mL distilled water, and then 10 mL ethanol solution of 1,10-phenanthroline was added dropwise (Fe : phenanthroline = 1 : 3 molar ratio), the reaction mixture was stirred at 60 °C for 2 h. Subsequent operations were similar to our previous work.[28] The obtained precursors were pyrolyzed at a heating rate of 5 °C min^{-1} in Ar atmosphere and held for 2 hours at 500 °C. Cooling naturally to room temperature, the catalysts were washed by distilled water. Herein, five iron salts are $FeCl_2 \cdot 4H_2O$, $FeCl_3 \cdot 6H_2O$, $FeSO_4 \cdot 7H_2O$, $Fe(NO_3)_3 \cdot 9H_2O$ and $Fe(acac)_3$, and the corresponding catalysts were denoted as Fe-NC-X (X = $FeCl_2$, $FeCl_3$, $FeSO_4$, $Fe(NO_3)_3$ and $Fe(acac)_3$), respectively. By comparison, the catalyst Fe–C was prepared by direct pyrolysis of a mixture of iron salts, baking soda and wheatmeal. Similar procedure was applied to prepare the sole NC without metal salts.

Characterization

The X-ray diffraction (XRD) patterns were gained by Mini Flex 600 using a Cu Kα X-ray source (40 kV, 100 mA) in the range of 5–80° with a scan rate of 4° min^{-1}. Raman spectra were performed with DXR Microscope at room temperature. Transmission electron microscopy (TEM) observations were performed on Tecnai G2 F20 high resolution analytical electron microscope operating at an acceleration voltage of 200 kV. Scanning electron microscopy (SEM) images were obtained by Hitachi S-4800 microscope. X-ray photoelectron spectroscopy (XPS) measurements were carried out on a PHI 1600 spectrometer with a Mg Kα X-ray source for excitation. The inductively coupled plasma optical emission spectrometer (ICP-OES) analysis were performed on VISTA-MPX. Elemental analysis (EA) was conducted on VarioEL cube elemental analyzer. N_2 adsorption–desorption experiments were performed on NOVA 2000e analyzer (Quantachrome, U.S.A.) at a liquid nitrogen temperature.

Catalyst evaluation

Transfer hydrogenation of nitrobenzene with FA. 0.25 mmol of nitrobenzene, 0.75 mmol of formic acid, 30 mg of catalyst, 1 mL of THF, and 1 mL of H_2O were added to 25 mL autoclave with a Teflon liner, flushing 3 times with nitrogen to remove air and pressurizing to 1 MPa. The reaction was performed at 120 °C for 6 h with magnetically stirred. After cooling down to room temperature, reaction liquid was filtered and analyzed by GC. After the reaction, Fe-NC-$FeCl_2$ was collected by simple magnetic separation and washed with ethanol several times for next cycle.

Results and discussion

As described above, a series of Fe-NC-X (X = $FeCl_2$, $FeCl_3$, $FeSO_4$, $Fe(NO_3)_3$, $Fe(acac)_3$) catalysts were obtained by pyrolysis of iron–phenanthroline complexes together with biomass carbon source. Their compositions and structures were characterized systematically.

As shown in Fig. 1a, XRD patterns of all Fe-NC-X catalysts were similar, indicating similar phase composition. Diffraction peaks at 29.9, 35.3, 42.8, 53.2, 56.7, 62.2° demonstrate the presence of Fe_3O_4. The broad peak at ~20° is ascribed to the amorphous carbon induced by relatively low pyrolysis temperature. It is markedly different from many previously reported examples, in which a sharp peak appeared corresponding to graphitic carbon, as a result of higher pyrolysis temperature.[32,33]

The Raman spectra of all catalysts are represented in Fig. 1b, in which D band (~1350 cm^{-1}) indicates the defect and vacancy

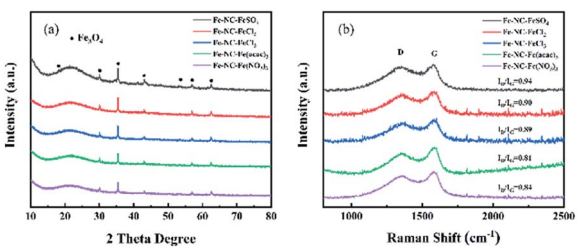

Fig. 1 (a) X-ray diffraction patterns and (b) Raman spectra of Fe-NC-X.

of material edge and G band (~1580 cm^{-1}) spawned by in-plane vibration of the sp^2 carbon atoms.[34] There are slight differences among the relative intensity ratio of D to G band (I_D/I_G) for all catalysts, demonstrating iron salts have no obvious effect on degree of graphitization. Moreover, the hump-like spectra of all catalysts suggests the presence of amorphous carbon, which is agreed well with XRD results.

Scanning electronic microscopy (SEM) and transmission electron microscopy (TEM) technique were employed to investigate the morphology of catalysts. We can found the particular sponge-like porous architecture for all samples (Fig. S1†), suggesting the important pore-creating role of $NaHCO_3$ in constructing porous morphology during pyrolysis process.[28]

The TEM images (Fig. 2) reveal that Fe_3O_4 nanoparticles dispersed on the carbon matrix in all Fe-NC-X catalysts. Nevertheless, it is worth noting that the particle sizes of Fe_3O_4 are extremely different from each other. The average particle sizes of Fe_3O_4 in Fe-NC-Fe$(NO_3)_3$, Fe-NC-$FeCl_2$, Fe-NC-$FeCl_3$ and Fe-NC-Fe$(acac)_3$ are 38.10 nm, 5.54 nm, 4.58 nm and 6.22 nm, respectively. In Fe-NC-$FeSO_4$, it can be found a broad diameter distribution of the Fe_3O_4 NPs, apart from a large proportion of relatively larger Fe_3O_4 particles up to ~130 nm, small particles ~5 nm dispersed rarely in the porous carbon matrix. The largest particle size in Fe-NC-$FeSO_4$ may be due to the stronger electrostatic interaction between SO_4^{2-} and iron than other anions, which may cause that the decomposition of iron species during pyrolysis become more difficult and higher temperature is required.[23] Firstly, iron sulfate agglomerates at lower temperature, and then decomposes to form larger nanoparticles at higher temperature, eventually lead to larger particle size of the NPs in Fe-NC-$FeSO_4$ catalyst. Meanwhile, no graphitic shells were found around Fe_3O_4 NPs for all samples. This can be due to low graphitization degree of carbon matrix at low pyrolysis temperature. In this respect, TEM results agree well with XRD and Raman characterizations.

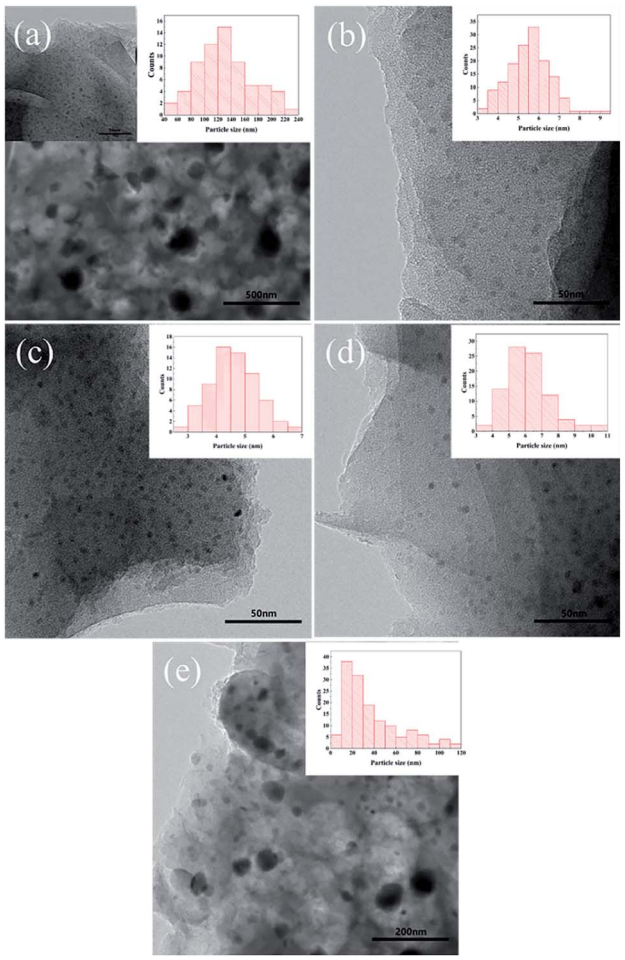

Fig. 2 TEM images of (a) Fe-NC-$FeSO_4$, (b) Fe-NC-$FeCl_2$, (c) Fe-NC-$FeCl_3$, (d) Fe-NC-Fe$(acac)_3$ and (e) Fe-NC-Fe$(NO_3)_3$.

The element compositions of all Fe-NC-X catalysts were detected by EA and ICP-OES analyses. According to Table 1, the element compositions of all catalysts are similar. Among them, Fe content of Fe-NC-$FeCl_2$ was determined as the highest (6.70%), while the Fe loading of Fe-NC-$FeCl_3$ was the lowest. No significant differences in N content were observed because of identical nitrogen source and pyrolysis temperature. Hence, the Fe salts cannot obviously influence element composition of the pyrolyzed catalyst. The N_2 adsorption/desorption isotherm of Fe-NC-X was measured to study the surface area, pore size and pore volume, according to Table S1,† the specific surface area and pore property of catalysts are not decisive to their catalytic activity which was presented in reported literature about carbon materials.[35,36]

The chemical state of nitrogen was investigated by XPS. The N 1s spectra shown in Fig. 3 exhibit four peaks with binding energy of 398, 399.4, 400.2, and 402 eV, assigned to pyridinic N, Fe-N, pyrrolic N, and graphitic N, respectively.[37] As shown in Table S2,† the dominating species in all catalysts is pyridinic N, which exhibits the strongest basicity among the several types of N.

At this point, the transfer hydrogenation of nitrobenzene with formic acid was chosen as a model reaction to explore the catalytic performance of the as-prepared Fe-NC-X catalysts. In the reaction, except the target product aniline, a small amount of formanilide was detected, which is produced by the reaction of aniline and FA. As shown in Table 2, conversion of nitrobenzene does not occur without catalyst. When the reaction was conducted over NC, only 6.1% nitrobenzene conversion was achieved, indicating that Fe_3O_4 NPs serve as active sites for transfer hydrogenation. Furthermore, the catalyst without N doped (donated as Fe-C) gives 23.5% nitrobenzene conversion, the

Table 1 The elemental contents of Fe-NC-X

	EA			ICP
Samples	C (wt%)	H (wt%)	N (wt%)	Fe (wt%)
Fe-NC-$FeSO_4$	64.30	2.05	5.37	6.29
Fe-NC-$FeCl_2$	67.65	2.33	5.81	6.70
Fe-NC-$FeCl_3$	68.10	2.19	5.79	5.78
Fe-NC-Fe$(acac)_3$	66.69	2.33	5.63	5.96
Fe-NC-Fe$(NO_3)_3$	68.53	2.11	5.73	6.38

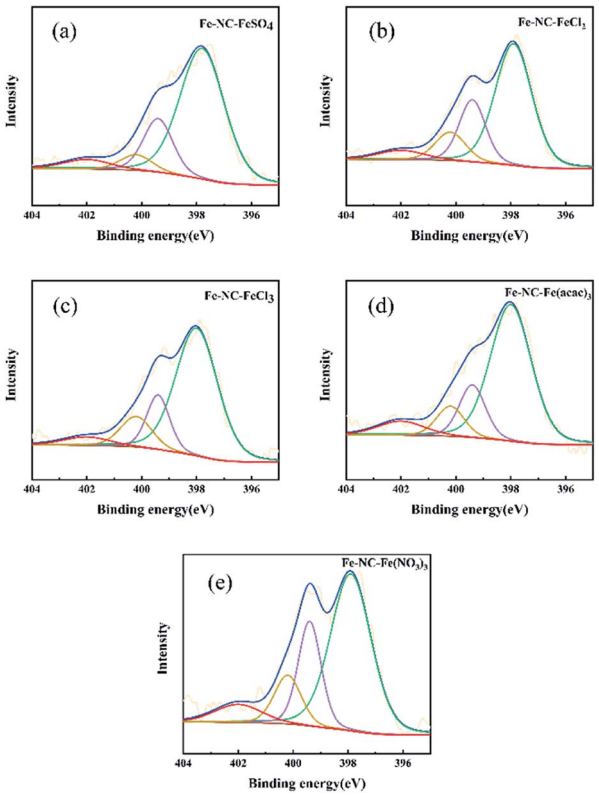

Fig. 3 N 1s XPS spectra of (a) Fe-NC-$FeSO_4$, (b) Fe-NC-$FeCl_2$, (c) Fe-NC-$FeCl_3$, (d) Fe-NC-Fe(acac)$_3$ and (e) Fe-NC-Fe$(NO_3)_3$.

sharp decrease in activity implies the influential role of nitrogen modification. Obviously, all Fe-NC-X catalysts exhibit CTH activities for nitrobenzene without extra base, meanwhile, metal species and N dopant are strictly required to afford the outstanding catalyst. However, the activities of Fe-NC-X are different. As presented comparison of nitrobenzene reduction in Table 2, Fe-NC-$FeCl_2$ gives best nitrobenzene conversion and aniline selectivity. The activities of Fe-NC-$FeCl_3$ and Fe-NC-Fe(acac)$_3$ are slightly lower than that of Fe-NC-$FeCl_2$. Fe-NC-$FeSO_4$ and Fe-NC-Fe$(NO_3)_3$ exhibited inferior behavior to the aforesaid three catalysts under identical reaction condition. Combined with the results of characterizations, the displayed catalytic activity follows the opposite order of particle size. Hence, we speculate that the major factor that affects CTH activity of Fe-NC-X catalysts is the size and dispersity of Fe_3O_4 NPs. According to TEM images, in Fe-NC-$FeSO_4$ the size and dispersity of Fe_3O_4 NPs is worst, so it exhibits the worst catalytic performance. Furthermore, the slight differences among the CTH activities of Fe-NC-$FeCl_2$, Fe-NC-$FeCl_3$, and Fe-NC-Fe(acac)$_3$ are probably caused by the Fe loadings. In Table S4,† we compare the reported catalysts for transfer hydrogenation of nitrobenzene, noble metal catalysts or homogeneous catalysts are usually employed together with basic additive. Compared with reported similar catalysts, our catalysts can exhibit excellent performance without any basic additive. This is attributed to doped pyridinic N species, which shows stronger basicity than other doped N species and endows the catalyst some basic properties.[38] It is believed to be beneficial to dissociate the O–H bond in formic acid,[30] hence leading to improved catalytic activity.

We have investigated the reduction abilities of Fe-NC-X using molecular hydrogen and the catalytic mechanism have been illustrated in our previous work.[28] The compared capacity of Fe-NC-X for catalytic hydrogenation is in accordance with CTH of nitrobenzene (Table S3†), but catalytic hydrogenation takes longer reaction time than CTH, implying similar active sites but different hydrogenation path. It could be concluded that nitrobenzene is reduced by *in situ* generated metal hydrides rather than molecular hydrogen decomposed by FA (Scheme 1). On the catalyst surface, abundant nitrogenous functional groups, especially for pyridinic N species, could function as Lewis-base sites,[39–42] behaving a similar role as that of base additives. The formic acid (hydrogen-donor) is absorbed on the basic sites, and then is removed proton by electron-rich nitrogen atoms to form $HCOO^-$, thus accelerating the transfer of hydrogen to metal NPs and the formation of metal hydrides. Hydrogen is transferred as metal hydrides intermediate and reacts with substrate absorbed on NPs. To sum up, the synergistic effect of doping N and Fe_3O_4 NPs is key factor for the activity of CTH.

Table 2 CTH results of nitrobenzene over different catalysts[a]

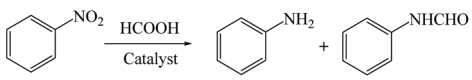

Entry	Catalyst	Conversion (%)	Selectivity (%)
1	No catalyst	—	—
2	Fe-NC-$FeSO_4$	62.7	90.3
3	Fe-NC-$FeCl_2$	98.0	97.1
4	Fe-NC-$FeCl_3$	96.7	84.9
5	Fe-NC-Fe(acac)$_3$	94.5	91.9
6	Fe-NC-Fe$(NO_3)_3$	82.7	94.1
7	NC	6.1	100
8	Fe-C	23.5	67.0

[a] Reaction conditions: nitrobenzene (0.25 mmol), FA (0.75 mmol), 30 mg of catalyst, solvent: 1 mL THF + 1 mL H_2O, 1 MPa N_2, 120 °C and 6 h.

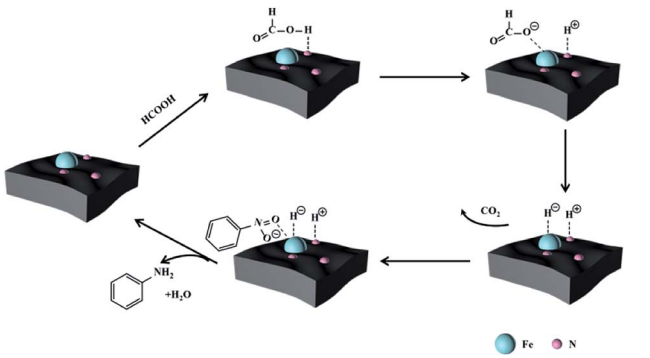

Scheme 1 Proposed mechanism for transfer hydrogenation of nitroarenes.

In order to demonstrate the general applicability of Fe-NC catalyst, reduction of various substituted nitroarenes were conducted under optimal reaction conditions. The performance of Fe-NC-$FeCl_2$ to convert nitroarenes to corresponding anilines is summarized in Table 3. It shows excellent performance for halogenated nitrobenzene, for example, fluoro-, chloro- and bromonitrobenzene are transformed into corresponding halogenated anilines with high yields. It is noteworthy that no dehalogenation occurring, which is of great significance in industrial production. For the substituted position, *o*- and *m*-nitrotoluene require longer time and more FA than *p*-nitrotoluene, it accounts for steric hindrance effect of the substituents. Besides, nitroanisole achieves complete conversion within 10 hours. To our delight, many reducible groups, such as aldehyde and nitrile, are well tolerated in the catalyst system, the multi-functional nitro-compounds can be selectively reduced to corresponding anilines in good yield with prolonged time. In addition, 6-nitroquinoline, which is poisonous for metal catalysts,[43] was efficiently converted to the corresponding aniline. In summary, the transfer hydrogenation of diverse nitroarenes to anilines occurred with excellent conversion and high selectivity, and no extra base was required in all cases above, indicating that the Fe-NC-$FeCl_2$ possesses good substrate tolerance for the nitro group reduction in the presence of diverse functional groups.

Finally, the stability and reusability of Fe-NC-$FeCl_2$ was investigated. The catalyst can be recovered by magnetic separation and washed with ethanol, and then it was reused for CTH of nitrobenzene in next cycle. Gratifyingly, our robust iron-based catalyst undergoes 5 times reuse without a significant drop of activity (Fig. S4†), revealing the good mechanical stability and acid-resistance of the catalyst, which provides possibility for the application in actual production.

Table 3 Catalytic transfer hydrogenation of substituted nitroarenes[a]

Entry	Substrate	Product	*t* (h)	Conv. (%)	Sel. (%)
1	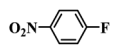	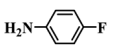	6	100	97.1
2	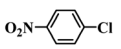	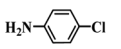	6	95.9	92.5
3	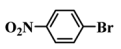	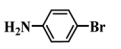	6	100	100
4	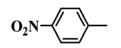	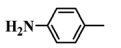	10	100	100
5[b]	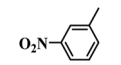	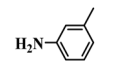	12	100	97.1
6[b]	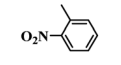	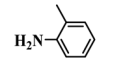	12	100	100
7	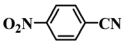	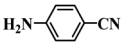	16	93.2	97.3
8[b]	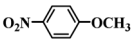	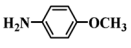	12	100	100
9[c]	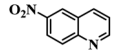	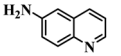	6	100	100
10	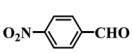	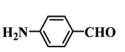	10	100	100

[a] Reaction conditions: nitro compounds (0.25 mmol), 30 mg of Fe-NC-$FeCl_2$, formic acid (0.75 mmol), 1 mL of H_2O and 1 mL of THF, 120 °C and 1 MPa N_2. [b] 3.5 eq. FA was added. [c] 130 °C.

Conclusions

In conclusion, we developed a series of Fe-based, N-decorated carbon catalysts *via* pyrolysis at 500 °C. The chemical composition and structural characterizations were measured by XRD, Raman Spectra, SEM, TEM, XPS, ICP and EA. The sponge-like porous catalysts were successfully applied to the transfer hydrogenation of nitro compounds with formic acid. According to the results of characterizations and experiments, Fe-NC-X catalysts exhibited different catalytic activity for transfer hydrogenation depending on the size and distribution of Fe-based NPs. Moreover, the reaction carried on efficiently without assistant of base additives owing to large amount of basic nitrogen sites of the catalysts. Among them, the catalyst Fe-NC-$FeCl_2$ with highest activity possesses small Fe_3O_4 NPs, more N doped, boosting the catalytic activity collectively. Particularly, the controllability of NPs' size and dispersion can be easily achieved by altering types of iron salts. Different iron salts lead to a variety of active particle size, thereby resulting in diverse catalytic activity. The versatile catalyst also affords excellent chemoselectivity towards various nitroaromatic containing multiple reducible groups. Moreover, the above catalyst was used for successive 5 runs, no obvious deactivation was observed.

Conflicts of interest

There are no conflicts to declare.

Acknowledgements

Financial support was provided by the National Natural Science Foundation of China (Grant No. 21808161).

Notes and references

1 S. K. Movahed, N. F. Lehi and M. Dabiri, *J. Catal.*, 2018, **364**, 69–79.
2 D. Formenti, F. Ferretti, F. K. Scharnagl and M. Beller, *Chem. Rev.*, 2019, **119**, 2611–2680.
3 J. Song, Z.-F. Huang, L. Pan, K. Li, X. Zhang, L. Wang and J.-J. Zou, *Appl. Catal., B*, 2018, **227**, 386–408.
4 Y. S. Dong and X. N. Fei, *Mater. Technol.*, 2020, **35**, 102–111.
5 G. D. Yadav and S. V. Lande, *Ind. Eng. Chem. Res.*, 2007, **46**, 2951–2961.
6 Y. G. Liu, Y. S. Lu, M. Prashad, J. Repic and T. J. Blacklock, *Adv. Synth. Catal.*, 2005, **347**, 217–219.
7 K.-i. Shimizu, Y. Miyamoto and A. Satsuma, *J. Catal.*, 2010, **270**, 86–94.
8 Z. Wei, J. Wang, S. Mao, D. Su, H. Jin, Y. Wang, F. Xu, H. Li and Y. Wang, *ACS Catal.*, 2015, **5**, 4783–4789.

9 X. Ma, Y. X. Zhou, H. Liu, Y. Li and H. L. Jiang, *Chem. Commun.*, 2016, **52**, 7719–7722.
10 H. Guo, B. Wang, P. Qiu, R. Gao, M. Sun and L. Chen, *ACS Sustainable Chem. Eng.*, 2019, **7**, 8876–8884.
11 M. Yuan, Y. Long, J. Yang, X. Hu, D. Xu, Y. Zhu and Z. Dong, *ChemSusChem*, 2018, **11**, 4156–4165.
12 R. I. Khan and K. Pitchumani, *ACS Sustainable Chem. Eng.*, 2018, **6**, 16130–16138.
13 H. T. Guo, R. X. Gao, M. M. Sun, H. Guo, B. W. Wang and L. G. Chen, *ChemSusChem*, 2019, **12**, 487–494.
14 A. Noschese, A. Buonerba, P. Canton, S. Milione, C. Capacchione and A. Grassi, *J. Catal.*, 2016, **340**, 30–40.
15 X. Cui, Y. Long, X. Zhou, G. Yu, J. Yang, M. Yuan, J. Ma and Z. Dong, *Green Chem.*, 2018, **20**, 1121–1130.
16 L. J. Jia, D. A. Bulushev, O. Y. Podyacheva, A. I. Boronin, L. S. Kibis, E. Y. Gerasimov, S. Beloshapkin, I. A. Seryak, Z. R. Ismagilov and J. R. H. Ross, *J. Catal.*, 2013, **307**, 94–102.
17 W. Wang, Q. Y. Jia, S. Mukerjee and S. L. Chen, *ACS Catal.*, 2019, **9**, 10126–10141.
18 R. V. Jagadeesh, A. E. Surkus, H. Junge, M. M. Pohl, J. Radnik, J. Rabeah, H. M. Huan, V. Schunemann, A. Bruckner and M. Beller, *Science*, 2013, **342**, 1073–1076.
19 R. V. Jagadeesh, K. Natte, H. Junge and M. Beller, *ACS Catal.*, 2015, **5**, 1526–1529.
20 J. Li, B. Wang, Y. Qin, Q. Tao and L. Chen, *Catal. Sci. Technol.*, 2019, **9**, 3726–3734.
21 L. Zhang, M. Zhou, A. Wang and T. Zhang, *Chem. Rev.*, 2020, **120**, 683–733.
22 Z. J. Li, D. H. Wang, Y. Wu and Y. D. Li, *Natl. Sci. Rev.*, 2018, **5**, 673–689.
23 R. X. Gao, H. T. Guo, B. W. Wang, P. Z. Qiu, M. M. Sun and L. G. Chen, *Appl. Catal., A*, 2019, **579**, 99–105.
24 X. Cui, Y. Li, S. Bachmann, M. Scalone, A. E. Surkus, K. Junge, C. Topf and M. Beller, *J. Am. Chem. Soc.*, 2015, **137**, 10652–10658.
25 R. V. Jagadeesh, H. Junge, M. M. Pohl, J. Radnik, A. Bruckner and M. Beller, *J. Am. Chem. Soc.*, 2013, **135**, 10776–10782.
26 F. A. Westerhaus, R. V. Jagadeesh, G. Wienhofer, M. M. Pohl, J. Radnik, A. E. Surkus, J. Rabeah, K. Junge, H. Junge, M. Nielsen, A. Bruckner and M. Beller, *Nat. Chem.*, 2013, **5**, 537–543.
27 R. V. Jagadeesh, K. Murugesan, A. S. Alshammari, H. Neumann, M.-M. Pohl, J. Radnik and M. Beller, *Science*, 2017, **358**, 326–332.
28 B. W. Wang, L. Liu, R. X. Gao, D. Zhang, Y. Li and L. G. Chen, *Int. J. Hydrogen Energy*, 2020, **45**, 1649–1657.
29 Y. F. Deng, Y. Xie, K. X. Zou and X. L. Ji, *J. Mater. Chem. A*, 2016, **4**, 1144–1173.
30 Y. Cao, S. Mao, M. Li, Y. Chen and Y. Wang, *ACS Catal.*, 2017, **7**, 8090–8112.
31 Y. Duan, T. Song, X. Dong and Y. Yang, *Green Chem.*, 2018, **20**, 2821–2828.
32 B. Sahoo, C. Kreyenschulte, G. Agostini, H. Lund, S. Bachmann, M. Scalone, K. Junge and M. Beller, *Chem. Sci.*, 2018, **9**, 8134–8141.
33 Y. Zhu, W. Sun, J. Luo, W. Chen, T. Cao, L. Zheng, J. Dong, J. Zhang, M. Zhang, Y. Han, C. Chen, Q. Peng, D. Wang and Y. Li, *Nat. Commun.*, 2018, **9**, 3861.
34 J. Song, Y. Ren, J. Li, X. Huang, F. Cheng, Y. Tang and H. Wang, *Carbon*, 2018, **138**, 300–308.
35 Y. Gao, G. Hu, J. Zhong, Z. Shi, Y. Zhu, D. S. Su, J. Wang, X. Bao and D. Ma, *Angew. Chem., Int. Ed. Engl.*, 2013, **52**, 2109–2113.
36 B. W. Wang, L. L. Si, J. Y. Geng, Y. H. Su, Y. Li, X. L. Yan and L. G. Chen, *Appl. Catal., B*, 2017, **204**, 316–323.
37 H. B. Wang, T. Maiyalagan and X. Wang, *ACS Catal.*, 2012, **2**, 781–794.
38 J. Y. Geng, L. L. Si, H. T. Guo, C. H. Lin, Y. Xi, Y. Li, X. L. Yan, B. W. Wang and L. G. Chen, *New J. Chem.*, 2017, **41**, 15447–15457.
39 M. F. R. Pereira, S. F. Soares, J. J. M. Órfão and J. L. Figueiredo, *Carbon*, 2003, **41**, 811–821.
40 Y. Wang, J. Yao, H. Li, D. Su and M. Antonietti, *J. Am. Chem. Soc.*, 2011, **133**, 2362–2365.
41 J. Long, K. Shen and Y. Li, *ACS Catal.*, 2016, **7**, 275–284.
42 J. Li, J. L. Liu, H. J. Zhou and Y. Fu, *ChemSusChem*, 2016, **9**, 1339–1347.
43 B. Sahoo, D. Formenti, C. Topf, S. Bachmann, M. Scalone, K. Junge and M. Beller, *ChemSusChem*, 2017, **10**, 3035–3039.

